

Article

# Degradation of Direct Blue 1 through Heterogeneous Photocatalysis with TiO<sub>2</sub> Irradiated with E-Beam

Elvia Gallegos<sup>1,2</sup>, Florinella Muñoz Bisesti<sup>3</sup> , Katherine Vaca-Escobar<sup>1</sup> , Cristian Santacruz<sup>4</sup>, Lenys Fernández<sup>1</sup> , Alexis Debut<sup>5</sup>  and Patricio J. Espinoza-Montero<sup>1,\*</sup> 

<sup>1</sup> Escuela de Ciencias Químicas, Pontificia Universidad Católica del Ecuador, Av. 12 de Octubre 1076, P.O. Box 17-01-2184, Quito, Ecuador; elvia.gallegosc@epn.edu.ec (E.G.); krvac@puce.edu.ec (K.V.-E.); lmfernandez@puce.edu.ec (L.F.)

<sup>2</sup> Departamento de Ingeniería Civil y Ambiental, Escuela Politécnica Nacional, Ladrón de Guevara E11-253, P.O. Box 17-01-2759, Quito, Ecuador

<sup>3</sup> Departamento de Ciencias Nucleares, Escuela Politécnica Nacional, Ladrón de Guevara E11-253, P.O. Box 17-01-2759, Quito, Ecuador; florinella.munoz@epn.edu.ec

<sup>4</sup> Departamento de Física, Escuela Politécnica Nacional, Ladrón de Guevara E11-253, P.O. Box 17-01-2759, Quito, Ecuador; cristian.santacruz@epn.edu.ec

<sup>5</sup> Centro de Nanociencia y Nanotecnología, Universidad de las Fuerzas Armadas ESPE, Av. Gral. Rumiñahui s/n, P.O. Box 171-5-231B, Sangolquí, Ecuador; apdebut@espe.edu.ec

\* Correspondence: pespinoza646@puce.edu.ec; Tel.: +593-2299-1700 (ext. 1929)

Received: 1 April 2020; Accepted: 7 September 2020; Published: 18 September 2020



**Abstract:** Most dyes used in the textile industry are chemically stable and poorly biodegradable, therefore, they are persistent in the environment and difficult to degrade by conventional methods. An alternative treatment for this kind of substance is heterogeneous photocatalysis using TiO<sub>2</sub>, so, in this work, it is proposed to degrade Direct Blue 1 (DB1) using microparticulate TiO<sub>2</sub> irradiated with e-beam at three different doses: 5, 10 and 20 kGy (J/kg). The DB1 degradation was implemented in a batch reactor (DB1 initial concentration = 50 mg L<sup>-1</sup>, pH 2.5, TiO<sub>2</sub> concentration = 200 mg L<sup>-1</sup>). We have demonstrated that the photocatalytic power of TiO<sub>2</sub>, when irradiated with e-beam (5, 10, 20 kGy), varies slightly, with minor effects on photodegradation performance. However, the dose of 10 kGy showed a slightly better result, according to the DB1 photodegradation rate constant. Adsorption process was not affected by irradiation; its isotherm was fitted to Freundlich's mathematical model. The DB1 photodegradation rate constants, after one hour of treatment, were: 0.0661 and 0.0742 min<sup>-1</sup> for irradiated (10 kGy) and nonirradiated TiO<sub>2</sub>, respectively. The degradation rate constant has an increase of 12.3% for irradiated TiO<sub>2</sub>. Finally, there was no evidence of mineralization in the degradation process after 60 min of treatment. According to the results, the irradiation of microparticulate TiO<sub>2</sub> with e-beam (10 kGy) slightly improves the photodegradation rate constant of DB1.

**Keywords:** Direct Blue 1; irradiated TiO<sub>2</sub>; heterogeneous photocatalysis; electron-beam; adsorption

## 1. Introduction

Effluents from the textile industry are considered an important environmental problem because it is difficult to treat due to their high nonbiodegradable load, partially attributed to the dye presence. At present, 100,000 different types of dyes are produced, of which about 36,000 tons dye/year are consumed by the textile industries [1]. The dyes are used in the dyeing stage, where up to 30% of them come off, becoming part of the industrial discharge [2].

Among the most used dyes are those of the azo type, which constitute around 70% of world production [3], due to their ease of preparation and the wide range of colors in which they are offered. These dyes have chromophore groups formed by double bonds –N=N– and have high stability to light

and washing. Most of them are sulfonic acids or their salts [4]. Its high stability determines properties of difficult degradation by conventional treatment methods; therefore, they are an important source of chemical and esthetic contamination [2]. Among the environmental problems caused by azo dyes are: color in effluents, visual pollution and eutrophication of water bodies, effects on gases solubility in water [5], generation of toxic, carcinogenic or mutagenic amines under specific conditions [6] and alterations in soil microbial biological activity of populations when they have been subjected to irrigation [7], among others.

One of the azo dyes used in the staining of denim fabrics in Ecuador, particularly in Pelileo (city located in the country center), is Direct Blue 1 (DB1), whose structure is shown in Figure 1, and it has two azo groups in its composition, it has a molecular weight of  $992.82 \text{ g mol}^{-1}$ , which resists temperatures of up to  $300 \text{ }^\circ\text{C}$ , and is difficult to degrade by conventional methods.

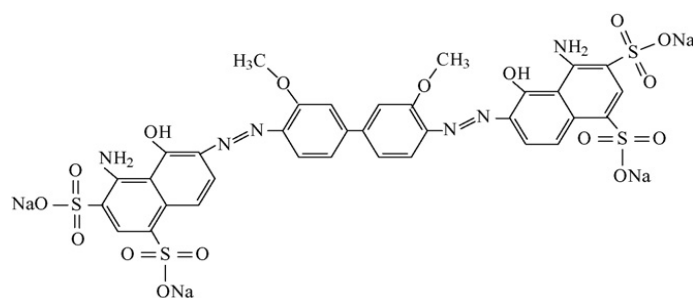


**Figure 1.** Direct Blue 1 (DB1) structure [8].

As an alternative treatment for compounds of difficult degradation, there are Advanced Oxidation Processes (AOPs), which are characterized by the oxidation reactions promoted by the hydroxyl radical ( $\bullet\text{OH}$ ) [9,10]. AOPs have been extensively studied for the oxidation of persistent compounds in water [11], such as dyes. Its advantages are simple handling, the relatively low cost of the reagents [9], as well as the oxidation of organic matter, even reaching its total mineralization ( $\text{CO}_2$ ,  $\text{H}_2\text{O}$  and inorganic salts) [1]. A brief summary of some AOPs and other methodologies used for DB1 degradation are shown in Table 1:

**Table 1.** DB1 degradation using Advanced Oxidation Processes (AOPs) and other methodologies.

Treatment	Operating Conditions	DB1 Concentration	Removal	Other Results	Ref.
Photocatalysis with C <sub>5</sub> N <sub>4</sub> irradiated	V = 20 mL; pH = 7; catalyst concentration = 100 mg L <sup>-1</sup> ; reactor batch.	50 mg L <sup>-1</sup>	Complete discoloration after 60 min of treatment	Low percentages of mineralization (10%)	[12]
Ozonation and electrocoagulation	V = 200 L, Q = 10 L min <sup>-1</sup> ; ozone injection = 5.21 mg min <sup>-1</sup> ; 1100 L tank capacity; $\frac{3}{4}$ in hydraulic line pipe. V = 1 L; electrode area = 160 cm <sup>2</sup> ; i = 5 mA cm <sup>-2</sup> ; aluminum anodes; iron cathodes.	50 mg L <sup>-1</sup>	50% color removal after 210 min 99% color removal after 20 min	Electrocoagulation is more economically viable than ozonation, since it promotes greater dye removal and requires less energy consumption	[13]
AOPs using pulsed corona discharge from water.	V = 300 mL; Q = 100 mL min <sup>-1</sup> , peroxide rate = $8.8 \times 10^{-4}$ mol L <sup>-1</sup> , pH = 3.5–10.3; conductivity = 100 $\mu$ S cm <sup>-1</sup>	10 mg L <sup>-1</sup>	75–80% color removal after 60 min.	The addition of hydrogen peroxide improves the discoloration rate.	[14]
Photocatalysis with TiO <sub>2</sub> films	V = 250 mL; pH = 2–10; 200 W mercury lamp	4–10 mg L <sup>-1</sup>	98% degradation after 1800 min at pH = 2	Decrease 12 to 46% removal of COD at a pH of 2 by varying dye concentration	[15]
Photocatalysis with TiO <sub>2</sub> and ZnO supported on polystyrene and polyethylene terephthalate	pH = 2.5 y 6 (TiO <sub>2</sub> ) y 7–11 (ZnO), 8 W UV lamps	50 mg L <sup>-1</sup>	100% degradation after 50 min with the two catalysts	The immobilized catalyst mass reached 0.399 mg cm <sup>-3</sup> for TiO <sub>2</sub> and 0.689 mg cm <sup>-2</sup> for ZnO in PET. The highest photocatalytic degradation was at pH = 2.5 using TiO <sub>2</sub> .	[16]
Photocatalytic degradation using rutile TiO <sub>2</sub>	-	-	Discoloration and removal of COD 60%	The rutile activity improves making a composite of it with polyaniline.	[17]
Photocatalysis with Fe <sub>2</sub> O <sub>3</sub> compounds, surrounded by C <sub>3</sub> N <sub>4</sub> and amorphous carbon.	V = 20 mL, T = 20 °C; pH = 7; catalyst mass = 50 mg; H <sub>2</sub> O <sub>2</sub> 30% solution; 35 W Xe lamp	500 mg L <sup>-1</sup>	Degradation greater than 99% after 50 min with C <sub>3</sub> N <sub>4</sub> and the same value after 35 min with the CN-Fe compound	TOC removal does not exceed 15%. Three cycle catalyst reuses with 99% removal results.	[18]
Peroxidase-mediated discoloration	H <sub>2</sub> O <sub>2</sub> concentration = 2.4 mM; nano enzyme concentration = 150 nM	10 $\mu$ M L <sup>-1</sup>	Complete discoloration of DB1 after three days.	-	[19]
Photocatalytic degradation with biogenic copper synthesized from native <i>Escherichia</i> sp.	V = 100 mL; catalyst mass = 100 mg; use of solar radiation	25–100 mg L <sup>-1</sup>	Discoloration of 88.42% after 5 h of exposure.	The concentrations of total dissolved solids, COD, hardness, chlorides, sulfates, electrical conductivity, total suspended solids, turbidity, and pH decreased.	[20]
Biosorptions using biomass of <i>Trametes versicolor</i>	V = 50 mL; biomass = 250 mg; pH = 2–9; T = 25 °C; batch system	25–800 mg L <sup>-1</sup>	Maximum biosorptions of 101.1 mg g <sup>-1</sup> for the native fungus and 152.3 mg g <sup>-1</sup> for the treated fungus.	Technology projection on a large scale.	[8]
Biotransformation by <i>Marinonacter</i> sp.	V = 100 mL; T = 37 °C; pH = 8; concentration NaCl = 70 g L <sup>-1</sup>	100 mg L <sup>-1</sup>	Complete discoloration after 6 h	Less toxicity of the metabolites with respect to the dye.	[21]
Adsorption, using low-cost adsorbents	V = 50 mL; T = 28 $\pm$ 2 °C; batch mode;	21%	Appreciable decrease in COD (70–90%) in samples treated for 1 h.	Cane bagasse is better absorbent than sawdust by 10% and brick dust by 25%	[22]
Discoloration by <i>Bacillus</i> sp.	NaCl concentration = 0–9%, pH = 5–9; T = 20–35 °C	150 mg L <sup>-1</sup>	47% discoloration after 24 h, 57% after 48 h and 73% after 72 h, all at pH = 7	The discoloration for the treatment in which the initial concentration was 25 mg L <sup>-1</sup> , was 25.10% and 29.51% higher, for 1 h and 5 h, respectively.	[23]
Degradation by laccase	V = 10 mL; laccase mass = 0.5 g; T = 30 °C	50 mg L <sup>-1</sup>	54 and 68% degradation for 18 h for the free and immobilized enzyme, respectively.	-	[24]
Discoloration by laccase from <i>Pycnoporus cinnabarinus</i>	V = 3.1 mL; pH = 4.9; laccase mass = 0.82–25 $\mu$ g	25 mg L <sup>-1</sup>	The disappearance of the dye is confirmed after contact with oxygen.	-	[25]
Degradation by azoreductase and laccase	-	0.6 mol L <sup>-1</sup>	80% discoloration after 24 h.	Production of toxic by-products in some cases, for example 3,3 dimethoxybenzidine in the case of DB1.	[26]
Adsorption using cement kiln powder	V = 250 mL, cement mass = g; Stirring speed = rpm	800 mg L <sup>-1</sup>	The removal is greater than the one carried out with activated carbon.	When washing the cement with colorant, it does not return to the water.	[27]

A widely used AOP is heterogeneous photocatalysis with  $\text{TiO}_2$ , which consists of an electron-hole pair ( $e^-$ - $h^+$ ) generation, by excitation of the electron from a semiconductor through UV radiation. The holes oxidize the hydroxyl ion in water to generate hydroxyl radicals ( $\bullet\text{OH}$ ), and electrons are transferred to adsorbed molecular oxygen to generate a superoxide ion. The  $\bullet\text{OH}$  generation allows the degradation of the target pollutant [10].

$\text{TiO}_2$  is a cheap, chemically stable, and nontoxic semiconductor. Several studies have been developed to improve its photocatalytic activity [28], for instance: doping with metal ions, doping with nonmetals, formation of compounds with  $\text{TiO}_2$  and with less energetic band gap semiconductors or with noble gases, dye sensitization, or rare earth modifications [10]. Some studies have applied ionizing radiation, particularly accelerated electrons (e-beam), to  $\text{TiO}_2$  nanoparticles, improving their photocatalytic activity [8,9]. There are few studies on this last modification, therefore, in this work the photocatalytic degradation of the DB1 dye is studied using a  $\text{TiO}_2$  microparticulate irradiated with accelerated electrons.

## 2. Materials and Methods

### 2.1. Reagents and Equipment

$\text{TiO}_2$  Hombitan (commercial grade, 325  $\mu\text{m}$  microparticulate) previously sieved, DB1 Dyetex, Quito-Ecuador and  $\text{H}_2\text{SO}_4$  1 N (Merck, Quito-Ecuador) were used. The equipment used was: ELU6U linear electron accelerator with 8 MeV power, EMPIREAN model PANanalytical diffractometer, Shimadzu TOC-5 total organic carbon meter, Hitachi U 1900, Tokio-Japan spectrophotometer, HACH 2800, Loveland-USA spectrophotometer, LABEC magnetic stirrer VELP, 15 W Sylvania Mercury.

### 2.2. $\text{TiO}_2$ Irradiation

A total of 2 g of  $\text{TiO}_2$  Hombitan by Venator Materials was placed in LDPE low-density polyethylene bags, and those bags were irradiated in a linear electron accelerator (ELU6U) at three doses: 5, 10 and 20 kGy (J/kg) [29,30].

### 2.3. $\text{TiO}_2$ Characterization

$\text{TiO}_2$  was characterized by X-Ray Diffraction (XRD), operating in a  $\theta$ -2 $\theta$  configuration (Bragg-Brentano geometry) equipped with a copper X-ray tube ( $K\alpha$ - $\lambda = 1.54056 \text{ \AA}$ ) at 45 kV and 40 mA. The diffractograms analysis was performed on the average of four measurements between the angles 5° to 90° ( $\theta$ -2 $\theta$ ) using the High Score Plus software.

Diffuse Reflectance Spectroscopy (DRS) was obtained at room temperature using a UV-VIS spectrometer equipped with an integrating sphere (Perkin Elmer, Lambda 365). The energy band gap of  $\text{TiO}_2$  samples was determined by extrapolating the slope to  $R \rightarrow 0$  in the plot  $(R/h\nu)^n$  versus  $h\nu$ , where  $R$  is the reflectance,  $h\nu$  is the photon energy and  $n = 2$  corresponds to direct allowed transitions [31–34]. The best fit to a straight line near the absorption edge was used to determine the energy band gap.

Infrared absorption of  $\text{TiO}_2$  powder samples was obtained by measuring the Fourier transform infrared (FTIR) in a Jasco FT/IR 4700 spectrometer. Samples were analyzed at room temperature in a region of 4000–400  $\text{cm}^{-1}$ . Spectral resolution was 1  $\text{cm}^{-1}$ . Adsorbed water was removed from  $\text{TiO}_2$  powder by heating the samples to 50 °C for 24 h.  $\text{TiO}_2$  powder was mixed with KBr and pressed into pellets.

Finally, elemental analysis by Energy-Dispersive X-ray Spectroscopy (EDS) was performed in a RESCAN MIRA 3 scanning electron microscope.

### 2.4. DB1 Degradation Tests with Irradiated $\text{TiO}_2$

The photocatalysis process was implemented in a batch reactor equipped with two Sylvania 15 W mercury lamps, with a working wavelength of 254 nm (UV region), two acrylic chambers and a water-cooling system (Figure 2), which allowed for keeping the temperature constant.

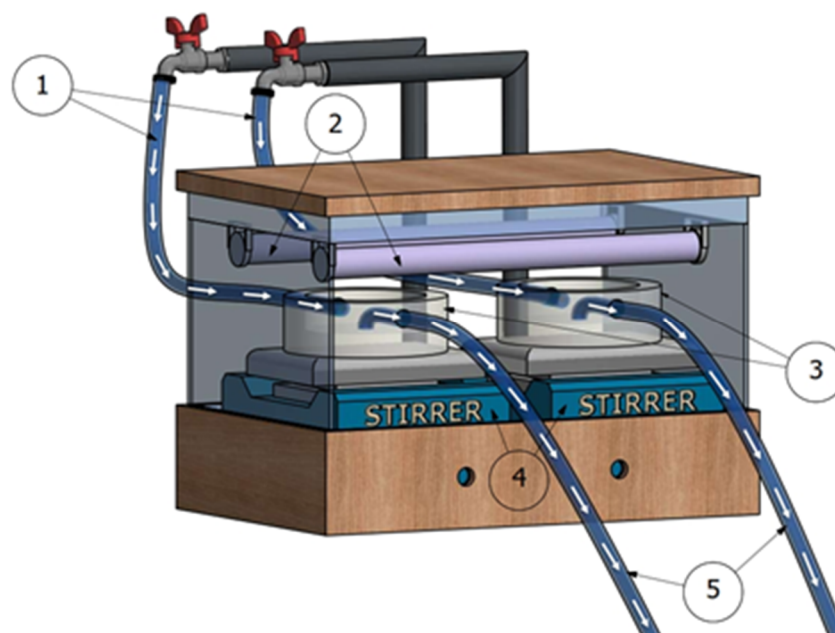


**Figure 2.** Diagram of the photoreactor used in the degradation of the DB1 dye. (1) Water inlet, (2) UV lamps, (3) Samples, (4) Magnetic stirrers, (5) Water outlet.

The effluent used was water with an initial concentration of  $50 \text{ mg L}^{-1}$  of DB1 dye, and  $200 \text{ mg L}^{-1}$  of both irradiated and nonirradiated  $\text{TiO}_2$  [16,17]. Then, ultrasound was applied for 10 min to the mixture.

Photodegradation was performed for 60 min, with stirring at 200 rpm [35] using a magnetic stirrer, Figure 2, and the change in pH was also followed by taking measurements at the beginning and at the end of the process. To verify degradation, aliquots were taken at different times, which were centrifuged (6000 rpm) to separate the catalyst from the sample. The sample was filtered through a Whatman filter with a pore diameter of  $0.45 \mu\text{m}$ . The DB1 concentration decrease was followed by spectrophotometry, at a wavelength of 565 nm [18]. The concentrations were obtained from a previously prepared calibration curve.

The DB1 degradation reaction constant was determined after one hour of photodegradation by fitting the experimental data to a kinetic model.

The irradiation dose effect on reaction rate was analyzed using a completely randomized design (CRD), the independent variable was irradiation dose and the response variable was the reaction constant. Statistical analyzes were developed in STATGRAPHICS Centurion XVIII software. The experiments were made in triplicate.

### 2.5. Adsorption Kinetics

DB1 adsorption in nonirradiated and irradiated  $\text{TiO}_2$  was studied for different doses (5, 10 and 20 kGy). This study was made using the Figure 2 reactor, in the same photodegradation conditions ( $C_{o, \text{DB1}} = 50 \text{ mg L}^{-1}$ ; catalyst dose =  $200 \text{ mg L}^{-1}$ ;  $\text{pH}_o = 2.5$ ;  $T_{\text{amb}}$ ) in light absence. Samples were taken every 10 min, during 50 min and were analyzed by spectrophotometry. With the experimental data of DB1 concentration, DB1 adsorption kinetics on  $\text{TiO}_2$  were determined, with which the adsorption equilibrium time was established.

### 2.6. Adsorption Isotherms

Solutions with different DB1 concentrations, in a range of 25 to  $250 \text{ mg L}^{-1}$ , were prepared. The conditions established in the previous section were used (Catalyst dose =  $200 \text{ mg L}^{-1}$ ;  $\text{pH} = 2.5$ ;  $T_{\text{amb}}$ ). Samples were taken after reaching the equilibrium time, previously determined, these samples were filtered through  $0.45 \mu\text{m}$  filters and measured by UV-vis spectrophotometry.

Experimental data were analyzed to identify if they fit Langmuir or Freundlich mathematical models, and the irradiation dose influence in adsorption onto  $\text{TiO}_2$  was studied using a CRD, in which the design variable was the irradiation dose (0 kGy and best dose) and the response variable was the best adjusted kinetic constant. Statistical analyzes were done in STATGRAPHICS Centurion XVIII software. The samples were taken in triplicate.

### 2.7. Contact Angles

The static contact angles were measured following the procedure described by [31–35]. Dried titanium dioxide samples were stored at ambient conditions before measurement.  $\text{TiO}_2$  powder was sprinkled uniformly on a  $2 \times 2$  cm clean flat surface. A glass microscope slide ( $20 \times 10 \times 2$  mm) was covered with double-sided adhesive tape. The tape was pressed to the powder with a 500 g weight for 10 s. The excess of powder was removed by using a razor blade. Finally, the slide was shaken to remove nonadhered material. This preparation technique produces a uniform powder surface. Measurements were taken immediately at ambient conditions,  $20^\circ\text{C}$  and 60% relative humidity. For the static contact angle, an 8  $\mu\text{L}$  droplet of deionized water was placed on the slide, and within 30 s three contact angle readings were measured (Dataphysics, OCA 25 equipped with electronic syringe module ESr-N). Each measurement was taken on three different positions of the slide and repeated on three slides. The average value is reported.

### 2.8. Mineralization Levels through TOC

Dye mineralization levels were measured at the beginning and ending of the process, through the determination of Total Organic Carbon (TOC), using method 5310 of the Standard Methods for the Examination of Water and Wastewater.

## 3. Results

### 3.1. X-ray Diffraction, Band Gap by DRS and FTIR Spectroscopy

Figure 3 show the two samples analyzed patterns ( $\text{TiO}_2$  nonirradiated and  $\text{TiO}_2$  irradiated).

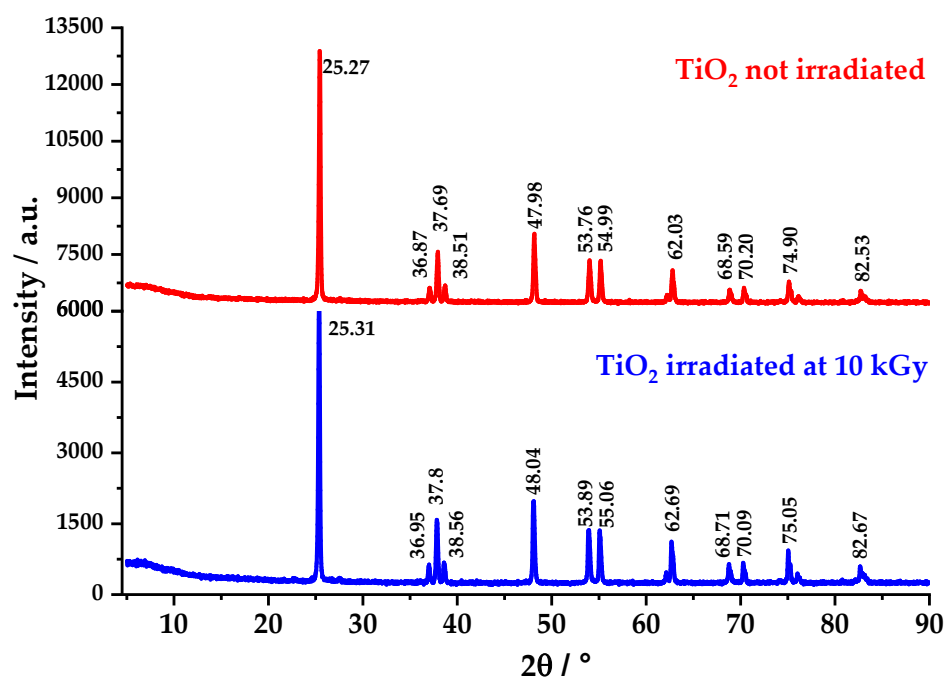
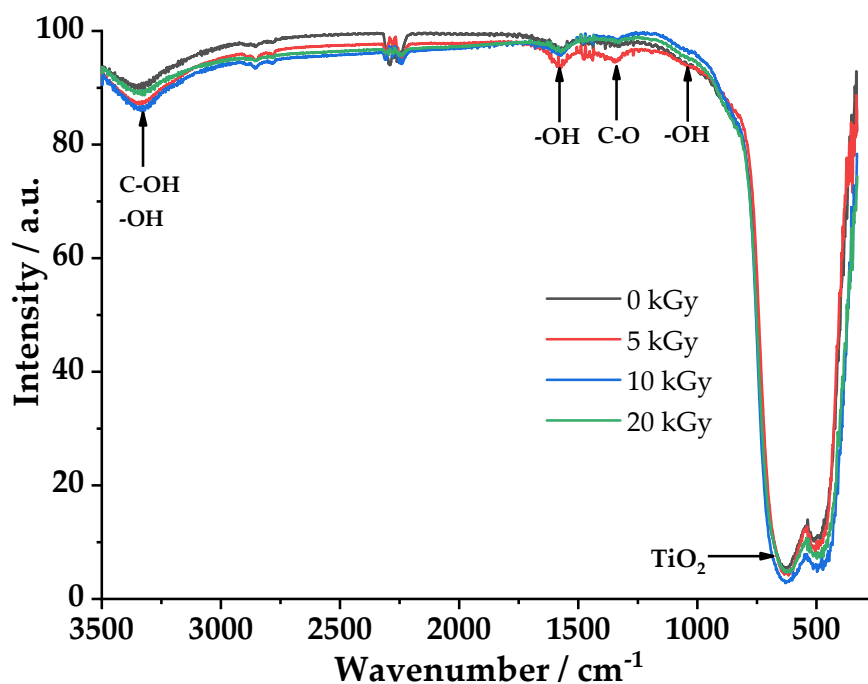


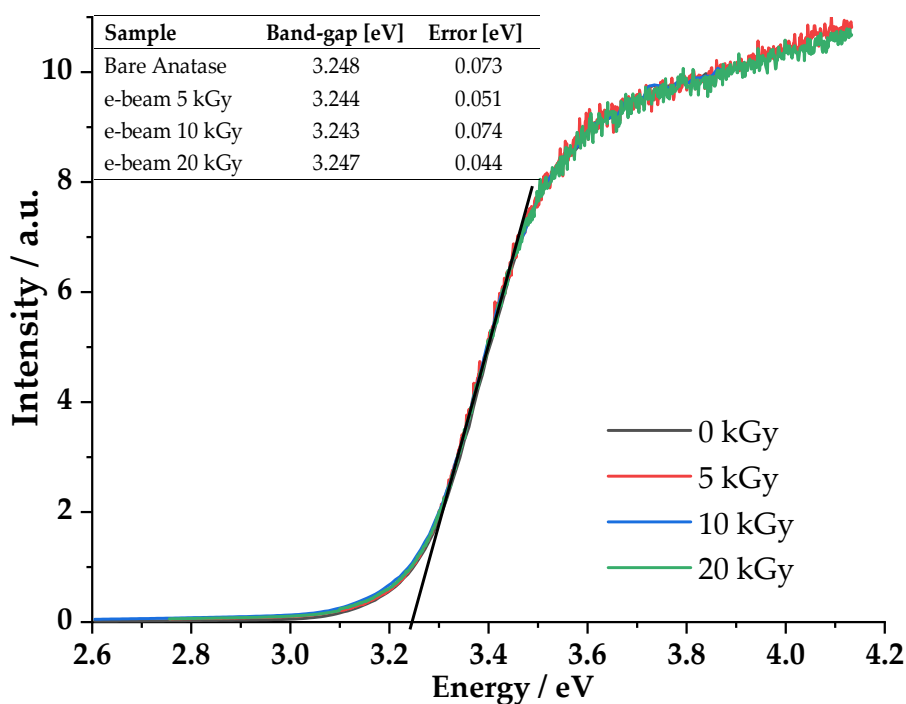
Figure 3.  $\text{TiO}_2$  X-ray diffraction with and without irradiation.

Figure 4 shows the FTIR spectra of TiO<sub>2</sub> samples, with and without e-beam treatment measured under ambient pressure conditions at the same humidity.



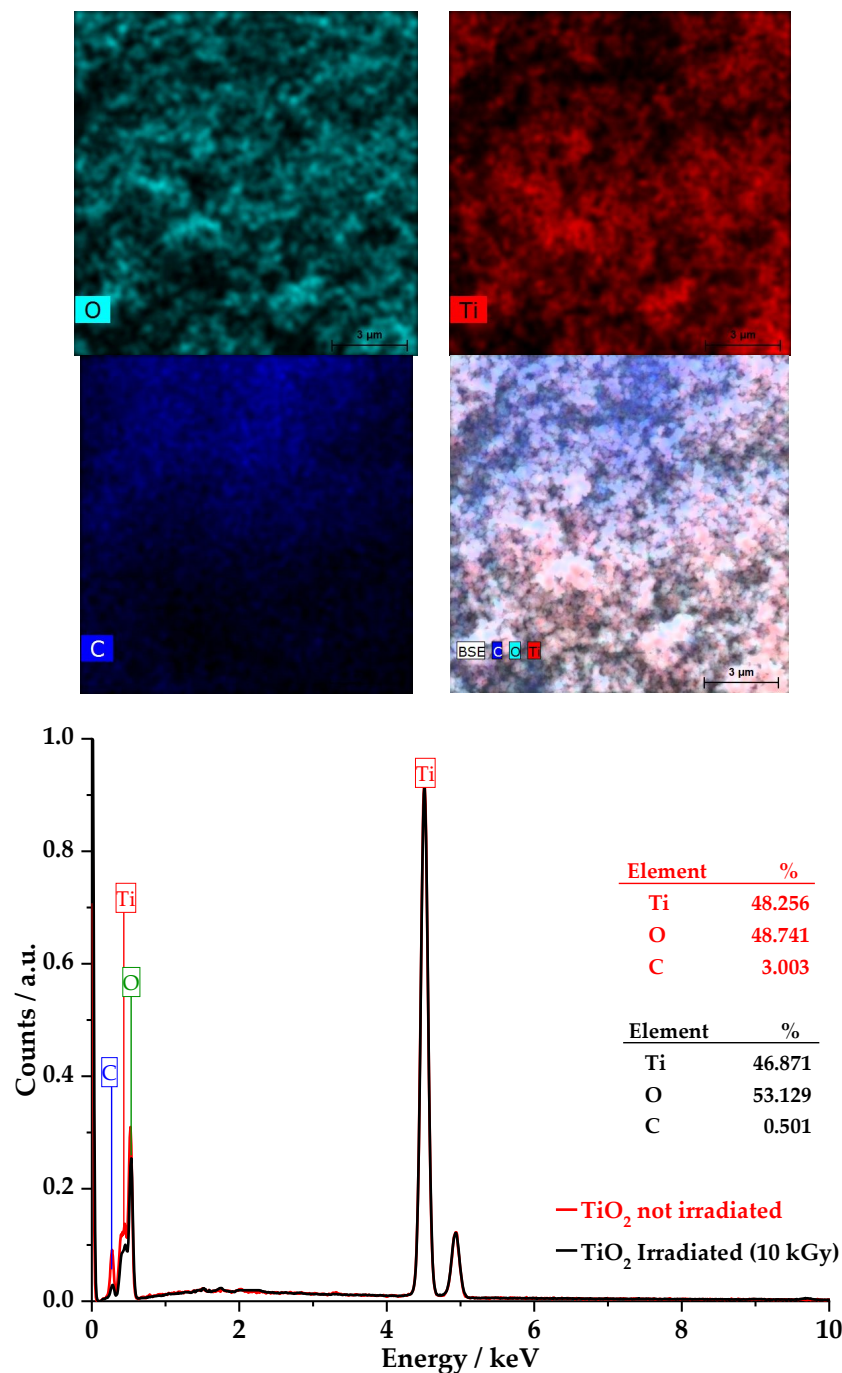
**Figure 4.** FT-IR spectra of TiO<sub>2</sub> with and without e-beam treatment measured under ambient conditions. Inset, a magnified view of the spectrum of the samples.

Band gap measurements were performed using DRS to determine if there were any changes in the optical properties of TiO<sub>2</sub> caused by e-beam treatment (5, 10, and 20 kGy) (Figure 5).



**Figure 5.** Diffuse Reflectance Spectroscopy (DRS) spectra of TiO<sub>2</sub> with and without e-beam treatment are displayed. Inset, the band gaps estimated from the DRS spectra are summarized.

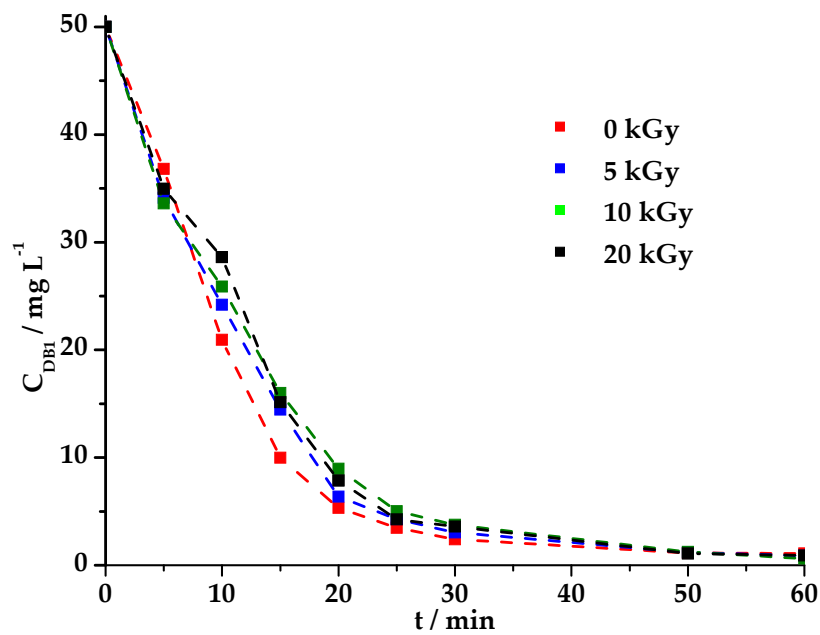
In order to verify the presence of C in the samples of  $\text{TiO}_2$ , EDS analysis was performed. Figure 6 shows an analysis based on mapping that identifies the elements that conform the sample. It is noted that the elements of the sample are O, Ti and C. The presence of C is attributed to the impurities in the sample. The averages of each element were 48.74%, 48.26%, and 3.00%, respectively.



**Figure 6.** Energy-Dispersive X-ray Spectroscopy (EDS) mapping of composition of sample of  $\text{TiO}_2$  without irradiation, and EDS spectrum of irradiated and unirradiated  $\text{TiO}_2$ .

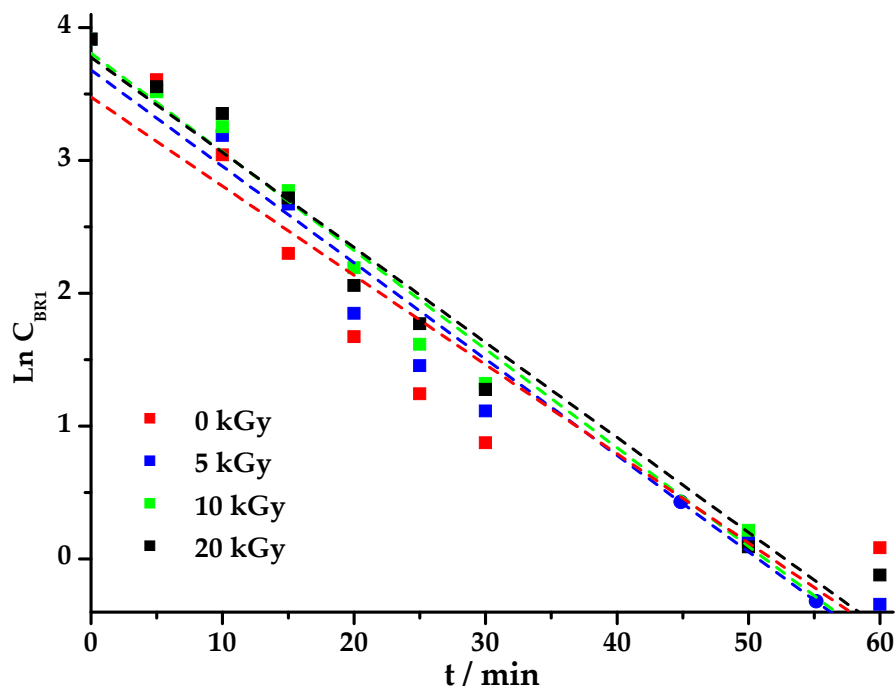
### 3.2. Heterogeneous Photocatalysis

The curves obtained from DB1 dye degradation by heterogeneous photocatalysis with  $\text{TiO}_2$  irradiated at various doses and nonirradiated are shown in Figure 7.



**Figure 7.** DB1 photodegradation on TiO<sub>2</sub> with and without e-beam treatment is displayed. Conditions:  $C_{0, DB1} = 50 \text{ mg L}^{-1}$ ; catalyst dose =  $200 \text{ mg L}^{-1}$ ;  $\text{pH}_0 = 2,5$ ;  $T_{\text{amb}} \approx 20 \text{ }^\circ\text{C}$ .

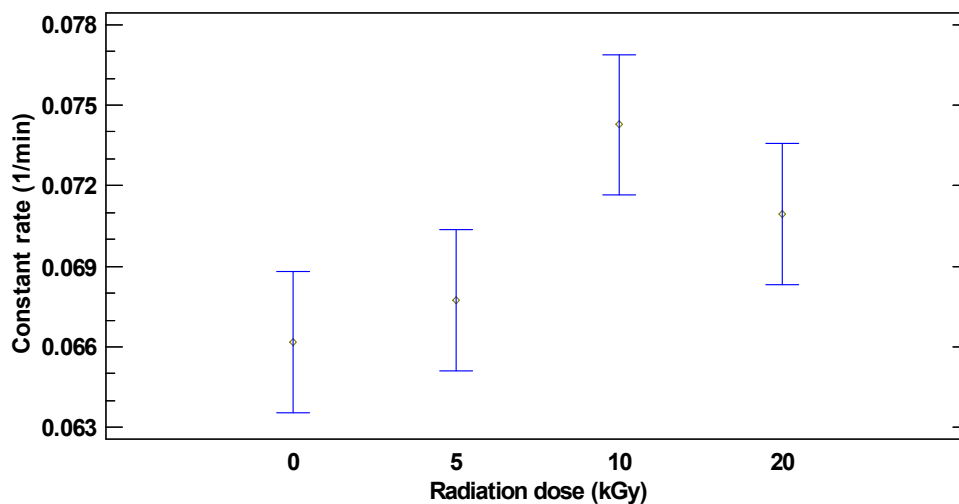
To determine the dye degradation reaction constants, a linear fit was performed as shown in Figure 8. The experimental data were adapted to a pseudo first order kinetic model which is consistent with what was reported in other studies [16,36]. Results are shown in Table 2. Subsequently, an ANOVA was performed (Figure 9) in order to analyze dye degradation constant rates.



**Figure 8.** DB1 linear adjustment according to pseudo first order kinetics, data from Figure 7.

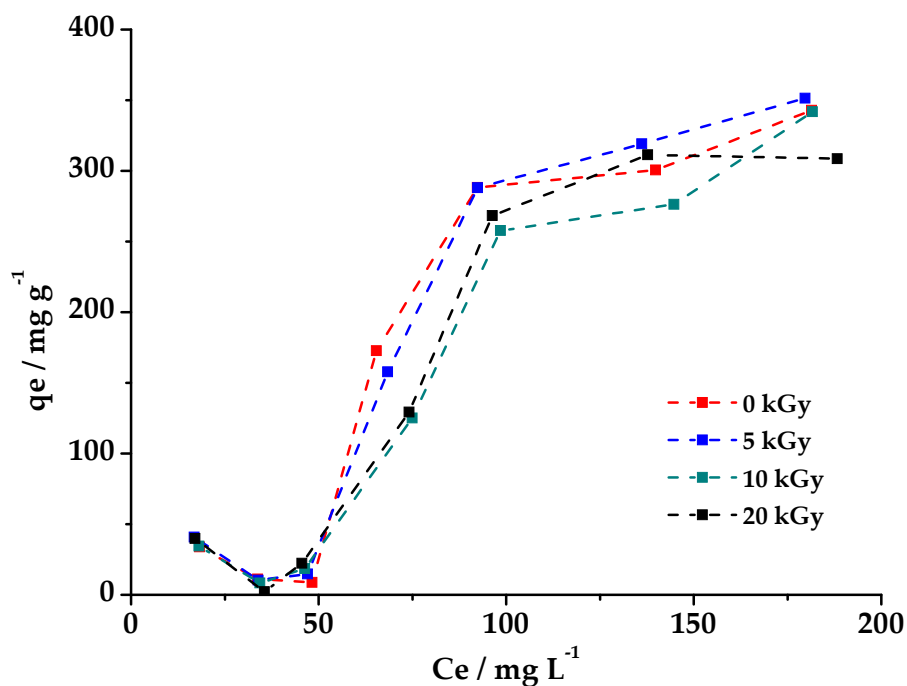
**Table 2.** Rate constants for pseudo first order reaction at different irradiation doses.

Radiation Dose (kGy)	Constant Rate	$r^2$
Not irradiated	0.0661	0.8826
5	0.0677	0.9273
10	0.0742	0.9818
20	0.0715	0.9644

**Figure 9.** Statistical analysis of irradiation dose effect on the photodegradation of DB1. Conditions:  $C_{o, DB1} = 50 \text{ mg L}^{-1}$ ; catalyst dose =  $200 \text{ mg L}^{-1}$ ;  $\text{pH}_o = 2.5$ ;  $T_{\text{amb}} \approx 20 \text{ }^\circ\text{C}$ .

### 3.3. Isotherms of Adsorption

Adsorption isotherms obtained were “S” type, they can be observed in Figure 10:

**Figure 10.** Adsorption DB1 dye isotherms of unirradiated and irradiated  $\text{TiO}_2$  at different doses (5, 10 y 20 kGy).

With increasing concentrations, isotherms took a trend that was later adapted to the Freundlich mathematical model (Equation (1)) with high correlations (Table 3). With the experimental data from this linearization, adsorption constant  $K_f$  was obtained for each adsorption dose. Their average values are detailed in Table 3. In addition, a statistical analysis of the  $K_f$  was performed using CRD as shown in Figure 11.

$$\log(Q_e) = \log(K_f) + \frac{1}{n} \log(C_e) \quad (1)$$

**Table 3.** Freundlich isotherm parameters.

Doses (kGy)	Parameters		
	$r^2$	$K_f$ ( $\text{mg g}^{-1}$ )	N
0	0.947	1.897	0.959
5	0.970	2.913	1.047
10	0.968	1.810	0.981
20	0.945	2.962	1.084

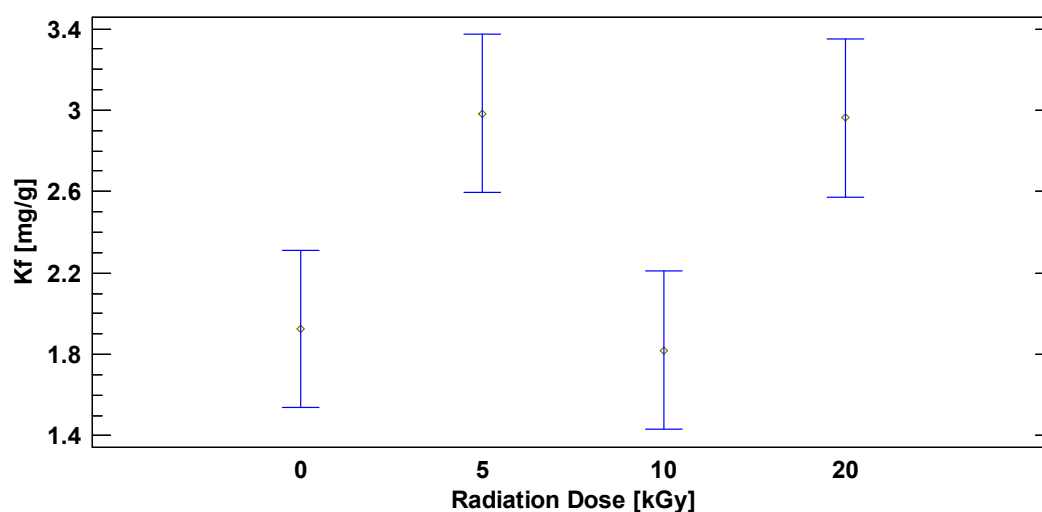


**Figure 11.** Statistical analysis of irradiation dose effect on DB1 adsorption. ( $C_{O, DB1} = 50 \text{ mg L}^{-1}$ ; catalyst dose =  $200 \text{ mg L}^{-1}$ ;  $\text{pH}_0 = 2.5$ ;  $T_{\text{amb}}$ ).

### 3.4. Mineralization

In Table 4, the percentages of DB1 mineralization levels achieved after one hour of treatment are presented.

**Table 4.** % Total Organic Carbon (TOC) removal during DB1 degradation after 60 min of treatment.

Doses kGy	%TOC
0	2.48
10	1.61

### 3.5. Contact Angles

The contact angle by sessile drop of the nonirradiated and irradiated  $\text{TiO}_2$  samples are shown in Figure 12 (insert).

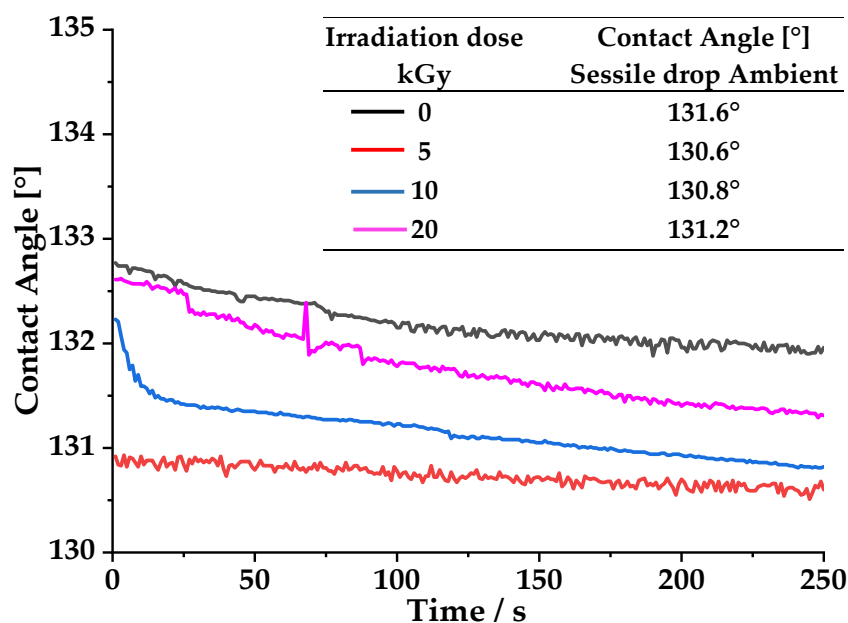


**Figure 12.** Contact angle by sessile drop without drying the sample (ambient), of the nonirradiated and irradiated TiO<sub>2</sub>. Insert, contact angle.

## 4. Discussion

### 4.1. X-ray Diffraction, Band Gap by DRS and FTIR Spectroscopy

Figure 3 shows TiO<sub>2</sub> X-ray diffraction patterns with and without irradiation. The main features of the XRD pattern of the two samples are similar, peaks at 25 and 48 degrees, which are anatase phase characteristic peaks [37], and it shows that the crystalline phase used for the photocatalyst when it was irradiated with accelerated electrons did not change. This result is in agreement with the ones found in other studies. A study has pointed out that there were no significant changes in the TiO<sub>2</sub> phase composition and crystal lattice when it was subjected to gamma irradiation at different doses (30–150 kGy) [38]. Another study shows that there were no changes in TiO<sub>2</sub> when it was irradiated with e-beam with an energy of 5 MeV and a current of 200 μA [39]. Also, the peaks in Figure 3 are in good agreement with the standard spectrum and XRD patterns were similar, indicating that there was no change in the crystallinity of TiO<sub>2</sub> caused by the e-beam treatment [39,40]. However, reports that changes in structure and improvement in photocatalytic activity were obtained at highest doses (5 MGy) [41].

The FTIR analysis results of the four TiO<sub>2</sub> samples with and without e-beam treatment, obtained under similar environmental conditions (same humidity), are shown in Figure 4. The samples treated at 5 and 10 kGy clearly show an increased signal corresponding to water. Signals at 3300, 1600 and 900 cm<sup>-1</sup> can be attributed to the OH-stretching, bending and vibrational water modes, respectively [42–44]. It is difficult to discriminate OH on C groups in IR spectra, because the C-O-H stretch overlaps the OH stretch of water adsorbed on the surface. However, in the electron beam-treated samples, especially at 5 kGy, the peak of the C–O stretching at 1400 cm<sup>-1</sup> is more intense, and this does not happen with other samples. This result was confirmed by the contact angle (Figure 12), where the sample treated at 5 kGy has the lowest contact angle (that is the highest wettability). In line with these results, it can be confirmed that the amount of water adsorbed on the TiO<sub>2</sub> surfaces increased after e-beam treatment, i.e., the TiO<sub>2</sub> surfaces became more hydrophilic [29]. Therefore, partial oxidation of C impurities on TiO<sub>2</sub> could be responsible for the slight improvement of photocatalytic activity. While, the TiO<sub>2</sub> reticular vibration signal can be assigned to the band between 600–700 cm<sup>-1</sup> [44]. The e-beam treatment had almost no influence on the geometric and electronic structures of TiO<sub>2</sub>.

To corroborate the presence of residual carbon in TiO<sub>2</sub>, from its synthesis, studies of EDS of the samples treated and not treated with e-beam were carried out. According to the results found,

the percentage of carbon decreased from 3.00% for the untreated sample to 0.50 % for the sample treated at 10 kGy (Figure 6). This leads us to presume that part of the impure C is released from the surface of TiO<sub>2</sub> with radiation, however this does not occur with the carbon that is within the TiO<sub>2</sub> crystalline structure. Apparently, the TiO<sub>2</sub> treatment with e-beam causes the carbon to acquire different oxidation states, which influences the photocatalytic behavior of TiO<sub>2</sub>.

Diffuse Reflectance Spectroscopy (DRS) was used to determine band gap, which was obtained by the Kubelka–Munk function. It was plotted as a wavelength function, where the intercept on the x-axis (energy) of the linear extrapolation of the Kubelka–Munk function corresponds to the material's band-gap (Figure 5) [45]. The energy band gap for all TiO<sub>2</sub> samples, irradiated and unirradiated, was around 3.25 eV (Insert of the Figure 5) which corresponds to reported value of anatase [34]. The value of the band gap does not change significantly up to irradiation, indicating that the change in optical properties cannot be the reason for the slight variation in photocatalytic activity. These results are consistent with those reported in the literature [29].

Furthermore, XPS studies reported by Kim M. J. et al., for the TiO<sub>2</sub> surface, show that Ti 2p spectra for untreated and e-beam-treated TiO<sub>2</sub> samples (5, 10, and 15 kGy) show no structural changes. In contrast, the C 1s spectrum was significantly influenced by the e-beam treatment, i.e., the existing C as an impurity underwent a noticeable structural change in front of the e-beam. Finally, it has been shown that when 5 and 10 kGy e-beam doses were used to irradiate TiO<sub>2</sub> samples, the absolute intensity of the C 1s state increases with respect to the untreated sample. The center of the C 1s peak shifts to a higher binding energy after e-beam treatment. In the case of e-beam exposure at 15 kGy, the intensity of the C 1s peak decreases. The change in C 1s state after e-beam treatment is due to the formation of C-O bonds, causing the TiO<sub>2</sub> surface to become more hydrophilic [29,46]. The literature is complemented by the results shown in this paper, with regard to contact angle, band gap, EDS and FTIR.

In the case of TiO<sub>2</sub> irradiated at 20 kGy, C 1s is removed, provoking a slightly decrease in the FTIR signals intensity and an increase in the contact angle (reduces hydrophilicity). The decrease of C 1s is due to the elimination of C by oxidizing agents created in the atmosphere by the e-beams and may become more dominant than the C deposition from the atmosphere, or oxidation of existing ones [29].

#### 4.2. Effect of Irradiation on Heterogeneous Photocatalysis

According to Figure 7, the degradation of the DB1 in the first 5 min is slightly faster in the case of TiO<sub>2</sub> irradiated at 10 kGy, however, after this time the degradation of the dye is slightly faster with nonirradiated TiO<sub>2</sub>. Unexpectedly, after 50 min of treatment, there is again a breaking point, where the irradiated TiO<sub>2</sub> becomes lighter faster. Therefore, a statistical analysis of the degradation rate constant is convenient, and it is shown later. A degradation of around 98% is reached for all cases at 60 min of treatment.

A linear fit was performed to determine the dye degradation rate constants, as shown in Figure 8. The experimental data were adapted to a pseudo first order kinetic model. The rate constant averages for three replications are detailed in Table 2. Subsequently, an ANOVA was performed, Figure 9, in which we determined that there is a statistically significant difference ( $p < 0.05$ ) in the reaction rate constants. This analysis indicates that the 10 kGy dose is the one that presents an improvement in the reaction rate constant, which is due an increase in the concentration of C-O bonds coming from impurities on the surface of TiO<sub>2</sub> [29].

#### 4.3. Effect of Irradiation Dose on Adsorption

The adsorption isotherms obtained were “S” type; that is, at low concentrations of adsorbate (DB1), the surface (TiO<sub>2</sub>) presents collateral associations, a process known as “cooperative adsorption” [47]. This kind of adsorption behavior implies a moderate intermolecular attraction between the adsorbate and the adsorbent, where there is a strong competition for the adsorption centers with solvent molecules or other adsorbates [48]. This process is identified in the isotherm as a turning point in the low concentration zone (Figure 10), as the adsorbate concentration increases, it presents better affinity

towards the surface, and can be seen as an increase in the curve slope until saturation of available sites is reached (maximum adsorption).

With increasing concentrations, isotherms take a trend that is later adapted to the Freundlich mathematical model with high correlations, Table 3. With the experimental data from this linearization, the adsorption constant  $K_f$  was obtained for each adsorption dose; this constant is an approximate indicator of the maximum adsorption capacity on  $\text{TiO}_2$  [49]. Their average values are detailed in Table 3.

Using a CRD, in which the independent variable was the irradiation dose and the response variable was the adsorption constant, it was determined that there was a statistically significant difference between these values ( $p < 0.05$ ). Figure 11 reflects that there is no a statistically significant difference between 0 and 10 kGy doses, nor between 5 and 20 kGy doses, but there is a statistically significant difference between 0 and 5 kGy doses, 0 and 20 kGy doses, 10 and 5 kGy doses, and between 10 and 20 kGy doses.

Particle size is a determining factor for the adsorption process, since it is related to the specific surface area, while the particle size decreases, the specific surface area increases and therefore, the number of active sites [50]. The  $\text{TiO}_2$  particle size used in this work was around 325  $\mu\text{m}$  (considered a micrometric size), which means that it could improve the adsorption capacity if the particle size decreases.

Nevertheless, an excessive adsorption might block the way of the light towards the nanoparticle and provoke a decrease in the photocatalytic efficiency, especially when there are big molecules such as DB1 [2]. This can be confirmed with the experimental results of  $K_f$ , for  $\text{TiO}_2$  without irradiation and  $\text{TiO}_2$  irradiated at 10 kGy, where the lowest value of  $K_f$  is obtained.

#### 4.4. Contact Angle

Contact angle refers to the angle that the surface of a liquid makes when it encounters a solid. The value of the contact angle depends mainly on the relationship between the adhesive forces between the liquid and the solid and the cohesive forces of the liquid. When the adhesive forces with the surface of the solid are very large in relation to the cohesive forces, the contact angle is less than 90 degrees, resulting in the liquid wetting the surface. Contact angle measurement is useful in the evaluation of surface macroscopic properties, such as surface energy and wettability [51].

The variation of the contact angle between irradiated and nonirradiated  $\text{TiO}_2$  samples is small. The e-beam produces a change on the surface that affects the contact angle variation, which goes down from 131.6° ( $\text{TiO}_2$ , 0 kGy) to 130.8° ( $\text{TiO}_2$ , 10 kGy), Figure 12; this slight decrease can be attributed to the increase in C-OH, as discussed above, which causes a slight increase of the wettability. That is likely related to the slight increase of the photocatalytic activity of the  $\text{TiO}_2$  irradiated at 10 kGy. However, studies show that to achieve a change in the oxidation state of Ti, an increase in the  $\text{Ti}^{3+}/\text{Ti}^{4+}$  ratio, and irradiation with an MeV electron beam is required [52]. There are some studies that compares the photocatalytic activity and the super-hydrophilicity of  $\text{TiO}_2$  induced by UV irradiation. The results are inconclusive, however, the composition and the processing of the material increases the photocatalytic activity and reduces the super-hydrophilic character, or vice versa [53–55]. According to Yu et al., the mechanism of photoinduced super-hydrophilicity of the films is different from that of photocatalytic oxidation, super-hydrophilicity is attributed to formation of surface trapped electrons and  $\text{Ti}^{3+}$  defective sites [56]. All these studies show that the photoinduced super-hydrophilicity is not permanent and reduces when the sample is stored in the dark for a couple of days.

#### 4.5. Mineralization

According to Table 4, the mineralization after 60 min of treatment with  $\text{TiO}_2$ , not irradiated and irradiated at 10 kGy, is very low. However, it is important to note that the interest of this research was not to achieve total mineralization, but to study the effect of irradiation on the degradation of the DB1. However, in a study developed with azo dyes, it was determined that total mineralization occurs at longer times, around 5 h [57], which means that this low percentage could be caused by the time taken

to mineralize the dye. Other studies attribute the low TOC to structure cleavage and to the production of organic molecular small fragments that are not fully mineralized under the prevailing oxidative conditions [58,59].

## 5. Conclusions

TiO<sub>2</sub> irradiated at 10 kGy allows a slightly faster degradation of DB1, compared to the degradation with TiO<sub>2</sub> irradiated at 0, 5, and 20 kGy; in this sense, the rate constant of degradation of DB1, on TiO<sub>2</sub> irradiated at 10 kGy, is slightly higher statistically, according to ANOVA analysis. The results of XRD and band gap are identical for the irradiated and unirradiated TiO<sub>2</sub> with e-beam, showing that e-beam irradiation show no changes in the crystalline structure of the TiO<sub>2</sub> samples. However, EDS and XPS results from similar e-beam irradiation show that its surface properties suffer slight modifications, and the residual carbon on the TiO<sub>2</sub> structure is oxidized by irradiation, forming oxygenated species (C-O), which causes an increase in the TiO<sub>2</sub> hydrophilicity. This was corroborated experimentally by decreasing the contact angle, increasing the FT-IR (signals to the C-OH). In the case of TiO<sub>2</sub> irradiated at 20 kGy, C-OH groups are lost; causing a decrease in the intensity of the corresponding signals in FTIR intensity and an increase in the contact angle (reduces wettability). Regarding the absorption, the TiO<sub>2</sub> irradiated at 10 kGy absorbs less than the other materials used (TiO<sub>2</sub> irradiated at 0, 5 and 20 kGy); this apparently slightly favors the degradation of DB1, since an excessive adsorption would prevent the adequate passage of light towards the photocatalyst, causing a decrease in the speed of the degradation.

**Author Contributions:** Conceptualization, P.J.E.-M. and F.M.B.; methodology, P.J.E.-M. and F.M.B.; software, K.V.-E., A.D. and C.S.; validation, E.G., F.M. and P.J.E.-M.; formal analysis, E.G., C.S. and A.D.; investigation, E.G.; resources, F.M.B. and P.J.E.-M.; data curation, K.V.-E.; writing—original draft preparation, E.G., P.J.E.-M., L.F. and F.M.B.; writing—review and editing, E.G., P.J.E.-M., K.V.-E., L.F. and F.M.B.; visualization, P.J.E.-M. and F.M.B.; supervision, P.J.E.-M. and F.M.B.; project administration, P.J.E.-M. and F.M.B.; funding acquisition, P.J.E.-M. and F.M.B. All authors have read and agreed to the published version of the manuscript.

**Funding:** This research was funded by ESCUELA POLITÉCNICA NACIONAL, grant number PIMI-14-13.

**Acknowledgments:** The authors wish to thank the Laboratorio de Investigaciones Aplicadas de la Escuela Politécnica Nacional for the support receive during this research and the Centro de Nanociencia y Nanotecnología, Universidad de las Fuerzas Armadas ESPE for the X-ray and EDS analysis.

**Conflicts of Interest:** The authors declare no conflict of interest.

## References

1. Reza, K.M.; Kurny, A.; Gulshan, F. Parameters affecting the photocatalytic degradation of dyes using TiO<sub>2</sub>: A review. *Appl. Water Sci.* **2017**, *7*, 1569–1578. [[CrossRef](#)]
2. Kordouli, E.; Bourikas, K.; Lycourghiotis, A.; Kordulis, C. The mechanism of azo-dyes adsorption on the titanium dioxide surface and their photocatalytic degradation over samples with various anatase/rutile ratios. *Catal. Today* **2015**, *252*, 128–135. [[CrossRef](#)]
3. Bafana, A.; Devi, S.S.; Chakrabarti, T. Azo dyes: Past, present and the future. *Environ. Rev.* **2011**, *19*, 350–371. [[CrossRef](#)]
4. Denisov, E.T.; Denisova, T.G.; Pokidova, T.S. *Handbook of Free Radical Initiators*; John Wiley & Sons: Hoboken, NJ, USA, 2005; ISBN 0471281832.
5. Nigam, P.; Banat, I.M.; Singh, D.; Marchant, R. Microbial process for the decolorization of textile effluent containing azo, diazo and reactive dyes. *Process Biochem.* **1996**, *31*, 435–442. [[CrossRef](#)]
6. Poyatos, J.M.; Muñoz, M.M.; Almecija, M.C.; Torres, J.C.; Hontoria, E.; Osorio, F. Advanced Oxidation Processes for Wastewater Treatment: State of the Art. *Water Air Soil Pollut.* **2010**, *205*, 187. [[CrossRef](#)]
7. Topaç, F.O.; Dindar, E.; Uçaroğlu, S.; Başkaya, H.S. Effect of a sulfonated azo dye and sulfanilic acid on nitrogen transformation processes in soil. *J. Hazard. Mater.* **2009**, *170*, 1006–1013. [[CrossRef](#)]
8. Bayramoğlu, G.; Arica, M.Y. Biosorption of benzidine based textile dyes “Direct Blue 1 and Direct Red 128” using native and heat-treated biomass of *Trametes versicolor*. *J. Hazard. Mater.* **2007**, *143*, 135–143. [[CrossRef](#)]

9. Oturan, M.A.; Aaron, J.-J. Advanced oxidation processes in water/wastewater treatment: Principles and applications. A review. *Crit. Rev. Environ. Sci. Technol.* **2014**, *44*, 2577–2641. [[CrossRef](#)]
10. Nevárez-Martínez, M.C.; Espinoza-Montero, P.; Quiroz-Chávez, F.; Ohtani, B. Fotocatálisis: Inicio, actualidad y perspectivas a través del TiO<sub>2</sub>. *Av. Química* **2017**, *12*, 45–59.
11. Daghrir, R.; Drogui, P.; Robert, D. Modified TiO<sub>2</sub> for environmental photocatalytic applications: A review. *Ind. Eng. Chem. Res.* **2013**, *52*, 3581–3599. [[CrossRef](#)]
12. Picho-Chillán, G.; Dante, R.C.; Muñoz-Bisesti, F.; Martín-Ramos, P.; Chamorro-Posada, P.; Vargas-Jentsch, P.; Sánchez-Arévalo, F.M.; Sandoval-Pauker, C.; Rutto, D. Photodegradation of Direct Blue 1 azo dye by polymeric carbon nitride irradiated with accelerated electrons. *Mater. Chem. Phys.* **2019**, *237*, 121878. [[CrossRef](#)]
13. Lambert, J.; Vega, M.M.; Isarain-Chavez, E.; Peralta-Hernandez, J.M. Ozone and electrocoagulation processes for treatment of dye in leather industry wastewater: A comparative study. *IJ Emerg. Technol. Adv. Eng.* **2011**, *3*, 1–9.
14. Sugiarto, A.T.; Ohshima, T.; Sato, M. Advanced oxidation processes using pulsed streamer corona discharge in water. *Thin Solid Films* **2002**, *407*, 174–178. [[CrossRef](#)]
15. Mohammed, A.K.; Mckenzie, K.T. Photocatalytic degradation of Chicago Sky Blue 6B and Benzopurpurin 4B using titanium dioxide thin film. *J. Environ. Sci.* **2005**, *17*, 869–872.
16. Sandoval, C.; Molina, G.; Jentsch, P.V.; Pérez, J.; Munoz, F. Photocatalytic degradation of azo dyes over semiconductors supported on polyethylene terephthalate and polystyrene substrates. *J. Adv. Oxid. Technol.* **2017**, *20*. [[CrossRef](#)]
17. Yazhini, K.B.; Savitha, K.U.; Prabu, H.G. Photocatalytic Degradation of Dyes using Rutile TiO<sub>2</sub>-Pani Composite Prepared by One Pot Method. *Environ. Pollut. Control Res.* **2014**, *1*, 1–6.
18. Dante, R.C.; Sánchez-Arévalo, F.M.; Huerta, L.; Muñoz-Bisesti, F.; Marquez, D.; Martín-Ramos, P.; Lartundo-Rojas, L.; Chamorro-Posada, P.; Solorza-Feria, O. Photocatalytic activity of a new composite material of Fe (III) oxide nanoparticles wrapped by a matrix of polymeric carbon nitride and amorphous carbon. *Fuller. Nanotub. Carbon Nanostruct.* **2017**, *25*, 630–636. [[CrossRef](#)]
19. ten Brink, H.B.; Dekker, H.L.; Schoemaker, H.E.; Wever, R. Oxidation reactions catalyzed by vanadium chloroperoxidase from *Curvularia inaequalis*. *J. Inorg. Biochem.* **2000**, *80*, 91–98. [[CrossRef](#)]
20. Noman, M.; Shahid, M.; Ahmed, T.; Niazi, M.B.K.; Hussain, S.; Song, F.; Manzoor, I. Use of biogenic copper nanoparticles synthesized from a native *Escherichia sp.* as photocatalysts for azo dye degradation and treatment of textile effluents. *Environ. Pollut.* **2020**, *257*, 113514. [[CrossRef](#)]
21. Prasad, A.S.A.; Satyanarayana, V.S.V.; Rao, K.V.B. Biotransformation of Direct Blue 1 by a moderately halophilic bacterium *Marinobacter sp.* strain HBRA and toxicity assessment of degraded metabolites. *J. Hazard. Mater.* **2013**, *262*, 674–684. [[CrossRef](#)] [[PubMed](#)]
22. Kaushik, C.P.; Tuteja, R.; Kaushik, N.; Sharma, J.K. Minimization of organic chemical load in direct dyes effluent using low cost adsorbents. *Chem. Eng. J.* **2009**, *155*, 234–240. [[CrossRef](#)]
23. Mahmood, F.; Shahid, M.; Hussain, S.; Shahzad, T.; Tahir, M.; Ijaz, M.; Hussain, A.; Mahmood, K.; Imran, M.; Babar, S.A.K. Potential plant growth-promoting strain *Bacillus sp.* SR-2-1/1 decolorized azo dyes through NADH-ubiquinone: Oxidoreductase activity. *Bioresour. Technol.* **2017**, *235*, 176–184. [[CrossRef](#)] [[PubMed](#)]
24. Karagoz, B.; Bayramoglu, G.; Altintas, B.; Bicak, N.; Arica, M.Y. Amine functional monodisperse microbeads via precipitation polymerization of N-vinyl formamide: Immobilized laccase for benzidine based dyes degradation. *Bioresour. Technol.* **2011**, *102*, 6783–6790. [[CrossRef](#)]
25. Schliephake, K.; Mainwaring, D.E.; Lonergan, G.T.; Jones, I.K.; Baker, W.L. Transformation and degradation of the disazo dye Chicago Sky Blue by a purified laccase from *Pycnoporus cinnabarinus*. *Enzym. Microb. Technol.* **2000**, *27*, 100–107. [[CrossRef](#)]
26. Mendes, S.; Farinha, A.; Ramos, C.G.; Leitão, J.H.; Viegas, C.A.; Martins, L.O. Synergistic action of azoreductase and laccase leads to maximal decolourization and detoxification of model dye-containing wastewaters. *Bioresour. Technol.* **2011**, *102*, 9852–9859. [[CrossRef](#)]
27. Saraya, M.E.-S.I.; Aboul-Fetouh, M.E.-S.; Nassar, H.S.; Abd-El-Rahman, A.M. Removal of direct dyes with cement kiln dust. *J. Mater. Sci. Eng. B* **2011**, *1*, 97.
28. Zaleska, A. Doped-TiO<sub>2</sub>: A review. *Recent Pat. Eng.* **2008**, *2*, 157–164. [[CrossRef](#)]
29. Kim, M.J.; Kim, K.-D.; Tai, W.S.; Seo, H.O.; Luo, Y.; Kim, Y.D.; Lee, B.C.; Park, O.K. Enhancement of Photocatalytic Activity of TiO<sub>2</sub> by High-Energy Electron-Beam Treatment Under Atmospheric Pressure. *Catal. Lett.* **2010**, *135*, 57–61. [[CrossRef](#)]

30. Latthe, S.S.; An, S.; Jin, S.; Yoon, S.S. High energy electron beam irradiated TiO<sub>2</sub> photoanodes for improved water splitting. *J. Mater. Chem. A* **2013**, *1*, 13567–13575. [[CrossRef](#)]
31. Köferstein, R.; Jäger, L.; Ebbinghaus, S.G. Magnetic and optical investigations on LaFeO<sub>3</sub> powders with different particle sizes and corresponding ceramics. *Solid State Ion.* **2013**, *249*, 1–5. [[CrossRef](#)]
32. Nowak, E.; Combes, G.; Stitt, E.H.; Pacek, A.W. A comparison of contact angle measurement techniques applied to highly porous catalyst supports. *Powder Technol.* **2013**, *233*, 52–64. [[CrossRef](#)]
33. Braginsky, L.; Shklover, V. Light absorption in TiO<sub>2</sub> nanoparticles. In *The European Physical Journal D*; Springer: Berlin, Germany, 1999; pp. 627–630.
34. Reddy, S.S.; Kotaiah, B. Decolorization of simulated spent reactive dye bath using solar/TiO<sub>2</sub>/H<sub>2</sub>O<sub>2</sub>. *Int. J. Environ. Sci. Technol.* **2005**, *2*, 245–251. [[CrossRef](#)]
35. Rodríguez Mora, J.A. *Estudio del Efecto del Uso de Dióxido de Titanio Asistido con Carbón Activado, Obtenido a Partir de un Residuo Industrial, en la Foto-Degradación del Colorante Azul BRL*; EPN: Quito, Ecuador, 2016.
36. Konstantinou, I.K.; Albanis, T.A. TiO<sub>2</sub>-assisted photocatalytic degradation of azo dyes in aqueous solution: Kinetic and mechanistic investigations. *Appl. Catal. B Environ.* **2004**, *49*, 1–14. [[CrossRef](#)]
37. Thamaphat, K.; Limsuwan, P.; Ngotawornchai, B. Phase characterization of TiO<sub>2</sub> powder by XRD and TEM. *Kasetsart J. (Nat. Sci.)* **2008**, *42*, 357–361.
38. Lamo, M.P.B.; Williams, P.; Reece, P.; Lumpkin, G.R.; Sheppard, L.R. Study of gamma irradiation effect on commercial TiO<sub>2</sub> photocatalyst. *Appl. Radiat. Isot.* **2014**, *89*, 25–29. [[CrossRef](#)]
39. Hou, X.G.; Gu, X.N.; Hu, Y.; Zhang, J.F.; Liu, A.D. Enhanced Pt/TiO<sub>2</sub> thin films prepared by electron beam irradiation. *Nucl. Instrum. Methods Phys. Res. Sect. B Beam Interact. Mater. At.* **2006**, *251*, 429–434. [[CrossRef](#)]
40. Hou, X.G.; Liu, A.D. Modification of photocatalytic TiO<sub>2</sub> thin films by electron beam irradiation. *Radiat. Phys. Chem.* **2008**, *77*, 345–351. [[CrossRef](#)]
41. Jun, J.; Dhayal, M.; Shin, J.H.; Kim, J.C.; Getoff, N. Surface properties and photoactivity of TiO<sub>2</sub> treated with electron beam. *Radiat. Phys. Chem.* **2006**, *75*, 583–589. [[CrossRef](#)]
42. Du, P.; Bueno-López, A.; Verbaas, M.; Almeida, A.R.; Makkee, M.; Moulijn, J.A.; Mul, G. The effect of surface OH-population on the photocatalytic activity of rare earth-doped P25-TiO<sub>2</sub> in methylene blue degradation. *J. Catal.* **2008**, *260*, 75–80. [[CrossRef](#)]
43. Warren, D.S.; McQuillan, A.J. Influence of adsorbed water on phonon and UV-induced IR absorptions of TiO<sub>2</sub> photocatalytic particle films. *J. Phys. Chem. B* **2004**, *108*, 19373–19379. [[CrossRef](#)]
44. Martra, G.; Coluccia, S.; Marchese, L.; Augugliaro, V.; Loddo, V.; Palmisano, L.; Schiavello, M. The role of H<sub>2</sub>O in the photocatalytic oxidation of toluene in vapour phase on anatase TiO<sub>2</sub> catalyst: A FTIR study. *Catal. Today* **1999**, *53*, 695–702. [[CrossRef](#)]
45. Sakthivel, S.; Kisch, H. Daylight Photocatalysis by Carbon-Modified Titanium Dioxide. *Angew. Chem. Int. Ed.* **2003**, *42*, 4908–4911. [[CrossRef](#)] [[PubMed](#)]
46. Moulder, J.F.; Stickle, W.F.; Sobol, P.E.; Bomben, K.D.; Chastain, J. *Handbook of X-ray Photoelectron Spectroscopy A Reference Book of Standard Spectra for Identification and Interpretation of XPS Data*; Physical Electronics: Chanhassen, MN, USA, 1995.
47. Giles, C.H.; Smith, D.; Huitson, A. A general treatment and classification of the solute adsorption isotherm. I. Theoretical. *J. Colloid Interface Sci.* **1974**, *47*, 755–765. [[CrossRef](#)]
48. Asenjo, V.N.G. *Una Nueva Generación de Carbones Activados de Altas Prestaciones Para Aplicaciones Medioambientales*. Ph.D. Thesis, Universidad de Oviedo, Oviedo, Spain, 2014.
49. Voudrias, E.; Fytianos, K.; Bozani, E. Sorption–desorption isotherms of dyes from aqueous solutions and wastewaters with different sorbent materials. *Glob. NEST Int. J.* **2002**, *4*, 75–83.
50. Zhang, Z.; Wang, C.-C.; Zakaria, R.; Ying, J.Y. Role of particle size in nanocrystalline TiO<sub>2</sub>-based photocatalysts. *J. Phys. Chem. B* **1998**, *102*, 10871–10878. [[CrossRef](#)]
51. Lamour, G.; Hamraoui, A.; Buvailo, A.; Xing, Y.; Keuleyan, S.; Prakash, V.; Eftekhari-Bafrooei, A.; Borguet, E. Contact angle measurements using a simplified experimental setup. *J. Chem. Educ.* **2010**, *87*, 1403–1407. [[CrossRef](#)]
52. Kim, M.S.; Jo, W.J.; Lee, D.; Baeck, S.; Shin, J.H.; Lee, B.C. Enhanced Photocatalytic Activity of TiO<sub>2</sub> Modified by e-Beam Irradiation. *Bull. Korean Chem. Soc.* **2013**, *34*, 1397–1400. [[CrossRef](#)]
53. Guan, K. Relationship between photocatalytic activity, hydrophilicity and self-cleaning effect of TiO<sub>2</sub>/SiO<sub>2</sub> films. *Surf. Coat. Technol.* **2005**, *191*, 155–160. [[CrossRef](#)]

54. Fujishima, A.; Rao, T.N.; Tryk, D.A. Titanium dioxide photocatalysis. *J. Photochem. Photobiol. C Photochem. Rev.* **2000**, *1*, 1–21. [[CrossRef](#)]
55. Lee, Y.C.; Hong, Y.P.; Lee, H.Y.; Kim, H.; Jung, Y.J.; Ko, K.H.; Jung, H.S.; Hong, K.S. Photocatalysis and hydrophilicity of doped TiO<sub>2</sub> thin films. *J. Colloid Interface Sci.* **2003**, *267*, 127–131. [[CrossRef](#)]
56. Jimmy, C.Y.; Yu, J.; Ho, W.; Zhao, J. Light-induced super-hydrophilicity and photocatalytic activity of mesoporous TiO<sub>2</sub> thin films. *J. Photochem. Photobiol. A Chem.* **2002**, *148*, 331–339.
57. Karkmaz, M.; Puzenat, E.; Guillard, C.; Herrmann, J.M. Photocatalytic degradation of the alimentary azo dye amaranth: Mineralization of the azo group to nitrogen. *Appl. Catal. B Environ.* **2004**, *51*, 183–194. [[CrossRef](#)]
58. Koch, M.; Yediler, A.; Lienert, D.; Insel, G.; Kettrup, A. Ozonation of hydrolyzed azo dye reactive yellow 84 (CI). *Chemosphere* **2002**, *46*, 109–113. [[CrossRef](#)]
59. Neamțu, M.; Zaharia, C.; Catrinescu, C.; Yediler, A.; Macoveanu, M.; Kettrup, A. Fe-exchanged Y zeolite as catalyst for wet peroxide oxidation of reactive azo dye Procion Marine H-EXL. *Appl. Catal. B Environ.* **2004**, *48*, 287–294. [[CrossRef](#)]



© 2020 by the authors. Licensee MDPI, Basel, Switzerland. This article is an open access article distributed under the terms and conditions of the Creative Commons Attribution (CC BY) license (<http://creativecommons.org/licenses/by/4.0/>).